NTM Excitation by Sawtooth Crashes and the Suppression of their Onset by Resonant Magnetic Perturbation

Q. Yu, S. Günter, K. Lackner, E. Strumberger, and V. Igochine
Max-Planck-Institut für Plasmaphysik, D-85748 Garching, Germany
Email contact of main author: qingquan.yu@ipp.mpg.de

Abstract. Numerical calculations based on the four-field equations have been carried to study (a) the triggering of neoclassical tearing modes (NTMs) by sawtooth crashes and (b) the effect of externally applied resonant magnetic perturbations (RMPs) on the growth of small magnetic islands. It is found that: (a) The destabilization of the *m/n=3/2* NTM by the *2/2* perturbations is most effective for large sawtooth amplitude, high plasma β value and low diamagnetic drift frequency, where m (n) is the poloidal (toroidal) mode number. The *3/2* magnetic perturbations first have the feature of an ideal mode and then show a tearing character later in time. (b) If the local bi-normal electron fluid velocity at the resonant surface is large enough, the growth of small *m/n=2/1* islands is suppressed by static 2/1 RMPs of moderate amplitude. The 4/2 or 6/3 component RMPs can also suppress the 2/1 island growth if the plasma rotation velocity is sufficiently large.

1. Introduction

Neoclassical tearing modes (NTMs) can degrade plasma confinement or even lead to disruptions in existing tokamak discharges. To understand (a) their triggering by sawtooth crashes and (b) the effect of externally applied resonant magnetic perturbations (RMPs) on their growth remain to be important for a fusion reactor. In this paper these two issues are studied numerically based on the four-field equations [1]. (a) The effects of the sawtooth amplitude, plasma β value and diamagnetic drift on mode coupling and the triggering of *m/n=3/2* NTMs by sawtooth crash are studied, indicating their important roles in affecting the *3/2* mode onset. (b) It is well known that large amplitude RMPs destabilize NTMs and cause mode locking. Moderate RMP amplitudes, however, have resulted in stabilized rotating magnetic islands in some experiments [e.g. 2,3]. Theoretical results based on a single-fluid model reveal that RMPs can cause a non-uniform island rotation and a net stabilizing effect [2,3]. Here the effects of electron diamagnetic drift and the associated ion polarization current are included, showing that the growth of originally unstable *m/n=2/1* islands is suppressed by RMPs of the same helicity at moderate amplitude if the local bi-normal electron fluid velocity is not too low. The plasma current density gradient at the resonant surface is found to be changed by RMPs [4].

2. Theoretical Model

A circular cross section of the equilibrium magnetic surfaces is assumed. The magnetic field is defined as [1]

$$\boldsymbol{B}=[(B_{0t}+b_t)/R]\boldsymbol{e}_t+\nabla\psi\times\boldsymbol{e}_t, \qquad (1)$$

where B_{0t} is the vacuum toroidal field, b_t is due to the diamagnetic correction, $\boldsymbol{e}_t$ is the unit vector along the toroidal direction, R the major radius, and ψ the flux function. The four-field equations, the electron continuity equation, generalized Ohm's law and the equation of motion in the perpendicular (after taking $\boldsymbol{e}_t\cdot\nabla\times$) and parallel direction, are utilized [1]. Normalizing the length to the plasma minor radius a, the time t to resistive time $\tau_R=a^2\mu_0/\eta$ (η is the plasma resistivity), the magnetic flux ψ to aB_{0t}, the ion velocity $\boldsymbol{v}$ to a/τ_R, and the electron density n_e to its value at the magnetic axis, these equations become [1, 4]

$$\frac{dn_e}{dt} = d_1(\nabla_{\parallel} j - \varepsilon\beta_e \frac{\partial(n_e + \phi/\Omega)}{\partial z}) - \nabla_{\parallel}(n_e v_{\parallel}) + \nabla\cdot(D_{\perp}\nabla n_e) + S_n, \quad (2)$$

$$\frac{d\psi}{dt} = E_0 - \eta(j - j_b) - \frac{\eta}{\nu_{ei}}\frac{dj}{dt} + \eta\frac{\mu_e}{\nu_{ei}}\nabla_{\perp}^2 j + \frac{T_e}{n_e}\Omega\nabla_{\parallel} n_e, \quad (3)$$

$$\frac{dU}{dt} = S^2(\nabla_{\parallel} j - \varepsilon\beta_e \frac{\partial n_e}{\partial z}) + \mu\nabla_{\perp}^2 U + S_m, \quad (4)$$

$$\frac{dv_{\parallel}}{dt} = -C_s^2\nabla_{\parallel} p/n_e + \mu\nabla_{\perp}^2 v_{\parallel}. \quad (5)$$

Differing from Ref. [1], the cold ion assumption is made, while the bootstrap current density j_b, electron inertia and viscosity are taken into account in Ohm's law (the 3rd - 5th terms in equation (3)). The ion velocity $v=\boldsymbol{v}_{||}+\boldsymbol{v}_{\perp}$, the subscripts || and $\perp$ denote the parallel and perpendicular components, $d/dt=\partial/\partial t+\boldsymbol{v}_{\perp}\cdot\nabla$, j is the toroidal plasma current density, $j_b=-c_b\sqrt{\varepsilon}(\partial p_e/\partial r)/B_p$, c_b a constant of order of unity, $\varepsilon=r/R_0$ the inverse aspect ratio, r the minor radius of the equilibrium magnetic surface, R_0 the major radius of the magnetic axis, z the coordinate along the vertical direction. T_e is the electron temperature, $p=p_e=n_eT_e$, and B_p the poloidal magnetic field. $U=-(R/R_0)^2\nabla_{\perp}^2\phi$ is the plasma vorticity, ϕ the stream function, μ (μ_e) the ion (electron) viscosity, and D the particle diffusivity. S_n and S_m are the particle and momentum sources, and E_0 is the equilibrium electric field. $S=\tau_R/\tau_A$, $d_1=\omega_{ce}/\nu_{ei}$, $\Omega=0.5\beta_e d_1$, $C_s=[T_e/m_i]^{1/2}/(a/\tau_R)$, and $\beta=\beta_e=8\pi n_eT_e/B_{0t}^2$, where ω_{ce} is the electron cyclotron frequency, υ_{ei} the electron-ion collisional frequency, $\tau_A=a/V_A$, and the Alfven velocity V_A is defined using B_{0t}.

The straight field line coordinate (r, θ, ζ) is utilized with the Jacobian $\sqrt{g}=rR^2/R_0$, where θ and ζ are the "poloidal-like" and toroidal angles [5]. The numerical code TM1 has been upgraded to include the toroidal coupling among modes with the same n but different m numbers, in addition to nonlinear two-fluid effects. The benchmark between TM1 and CASTOR-3D [6] indicates that the results from these two codes agree for $n>1$ modes if the β value is not too high.

The following equilibrium plasma parameters are used for the reference case: $B_{0t}=2T$, $a=0.5m$, $a/R_0=0.2$, $T_e=2keV$, and $n_e=3\times10^{19}m^{-3}$, leading to $S=2.6\times10^8$, $d_1=3.1\times10^7$, $C_s=2.0\times10^7 a/\tau_R$, $\tau_R=23s$, and $\nu_{ei}=2.2\times10^4/s$. Furthermore, $\mu_e/\upsilon_{ei}=10^{-4}a^2$, $\mu=0.2m^2/s=19a^2/\tau_R$, $D_{\perp}=\mu/50$, and a constant electron temperature are assumed. These input parameters are used for our calculations if not mentioned elsewhere.

In tokamak experiments the plasma rotation is essentially toroidal, while in Eqs. (2)-(5) due to the large aspect ratio approximation only the poloidal rotation is included, so that a larger plasma viscosity for the $m/n=0/0$ component, $\mu_{0/0}=18.8\times10^2(a^2/\tau_R)$, is used. This value guarantees a reasonable balance between the electromagnetic and viscous force, based on the following considerations [2]: (a) The electromagnetic force in the toroidal direction is smaller than that in the poloidal direction. (b) To have the same mode frequency due to the plasma rotation, the toroidal rotation velocity should be larger than the poloidal one. These two effects lead to a larger viscous force compared to the electromagnetic force for the toroidal rotation case by a factor $[(m/n)(R/r)]^2 \sim 10^2$.

3. Destabilization of m/n=3/2 NTMs by 2/2 Perturbations

A monotonic radial profile for the equilibrium safety factor q are assumed with $q_{r=0}=0.91$ and $r_{q=1}= 0.3a$, where $r_{q=1}$ is the minor radius at $q=1$ surface. The $q=3/2$ surface is at $r_{3/2} =0.68a$. A parabolic radial profile for the equilibrium electron density is taken. In order to understand the triggering of the $m/n=3/2$ mode by sawtooth crashes, we first look into the destabilization of a $3/2$ mode by a $2/2$ tearing mode, excluding $n=1$ perturbations. The components with the helicities $m/n=2/2$ and $3/2$ as well as those due to the toroidal mode coupling among other $n=2$ components are included in calculations. Without mode coupling, the $m/n=2/2$ (3/2) mode is unstable (stable) in the linear phase.

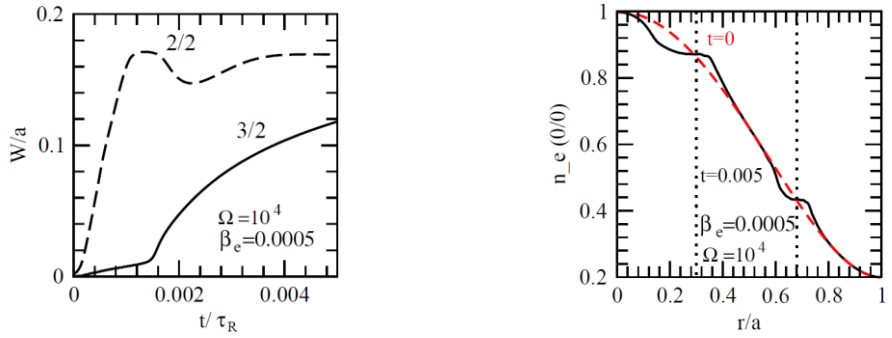

FIG. 1. (Left) Time evolution of the normalized 2/2 (dashed curves) and 3/2 (solid) island widths for $\beta_e=0.0005/\Omega=10^4$. (Right) Corresponding radial profiles of the normalized m/n=0/0 component electron density at t=0 and 0.005 τ_R. The vertical dotted lines show the locations of $r_{q=1}$ and $r_{3/2}$.

The electron diamagnetic drift frequency is proportional to the input parameter Ω in equation (3). For $\Omega=10^4$, one finds $\omega_{*e,2/2}=0.68\times10^5/\tau_R$ ($f_{*e,2/2}=0.47kHz$), $\omega_{*e,3/2}=1.2\times10^5/\tau_R$ ($f_{*e,3/2}=0.83kHz$) and $\Delta\omega_{*e}=(\omega_{*e,3/2}-\omega_{*e,2/2})=5.2\times10^4/\tau_R$, where $\omega_{*e,2/2}=2V_{*e}/r$ and $\omega_{*e,3/2}=3V_{*e}/r$ are calculated at $r_{q=1}$ and $r_{q=3/2}$, respectively. V_{*e} is the equilibrium electron diamagnetic drift velocity. For these parameters, the time evolution of the normalized $2/2$ (dashed curves) and $3/2$ (solid) island widths are shown in Fig. 1 (left). The "island width" $W_{m/n} =4[\psi_{m/n}/(B_p\, q/q')]^{1/2}$ is calculated at $r_{m/n}$, where $r_{m/n}$ and $\psi_{m/n}$ are the minor radius of the resonant surface and the perturbed flux of the m/n component. The $3/2$ mode is driven to grow by its coupling to the $2/2$ mode for a quite low β_e, $\beta_e=5\times10^{-4}$, due to a large $2/2$ island width and a small value of Ω. The bootstrap current density fractions are $f_b=0.066$ at $r_{q=1}$ and $f_b=0.2$ at $r_{3/2}$. Corresponding radial profiles of the normalized $m/n=0/0$ component electron density at $t=0$ and $0.005\,\tau_R$ are shown in Fig. 1 (right). The electron density flattens around the $q=1$ and 1.5 surfaces at $t= 0.005\,\tau_R$ due to the magnetic islands formed there.

Increasing the value of Ω to $\Omega=2\times10^4$ ($f_{*e,3/2}=1.7kHz$), the time evolution of the normalized $2/2$ (dotted curves) and $3/2$ (solid) island width is shown in Fig. 2 (left) by the black curves for $\beta_e=0.001$. It is seen that the $2/2$ mode grows first, and the $3/2$ mode grows later similar to the case shown in Fig. 1. For an even larger value of Ω, $\Omega=4\times10^4$ ($f_{*e,3/2}=3.3kHz$), and $\beta_e=0.007$, the $3/2$ mode grows first, but its amplitude oscillates in time around $t=0.001\,\tau_R$ before the island grows up to a large width. The $2/2$ mode is suppressed at the beginning but grows more quickly later (Fig. 2 left). For the latter case, the radial profiles of $\psi_{3/2}$ first show the feature of an ideal mode, with a small value of $\psi_{3/2}$ at $r_{3/2}$ (Fig. 2 right). The $n=2$ perturbations are however not shielded by the $q=3/2$ surface. At a later time the $\psi_{3/2}$ profiles have the feature of a tearing mode, although there is a local peak in the $\psi_{3/2}$ profile at $r_{3/2}$. The amplitudes of $\psi_{3/2}$ outside the $q=3/2$ surface are similar at the two different times although the island width is quite different. Such a feature is consistent with

experimental observations [7]. The black curves in Fig. 2 are obtained for $\beta_e=0.001/\Omega=2\times10^4$ at $t=3\times10^{-3}\,\tau_R$. In this case a "constant ψ" approximation for the tearing mode is valid due to a smaller value of Ω.

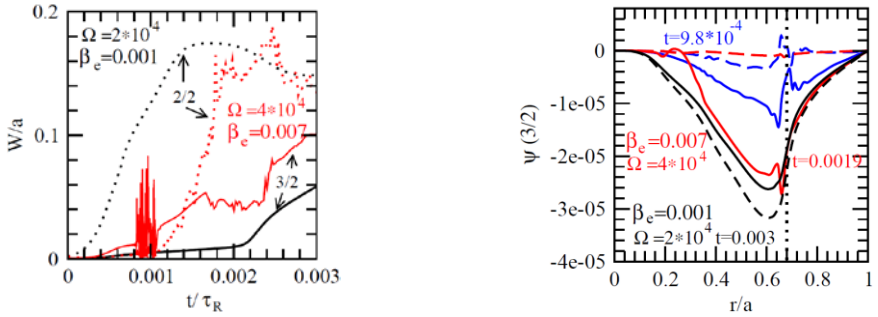

FIG. 2. (Left) Time evolution of the normalized 2/2 (dotted curves) and 3/2 island width (solid) with $\beta_e=0.001/\Omega=2\times10^4$ (black) and $\beta_e=0.007/\Omega=4\times10^4$ (red). (Right) Corresponding radial profiles of the normalized $\psi_{3/2}$ for $\beta_e=0.001/\Omega=2\times10^4$ at $t=3\times10^{-3}\,\tau_R$ (black) and for $\beta_e=0.007/\Omega=4\times10^4$ at $t=9.8\times10^{-4}\,\tau_R$ (blue) and $1.9\times10^{-3}\,\tau_R$ (red). The solid (dashed) curves are for the real (imaginary) parts. The vertical dotted line shows the location of $r_{3/2}$.

When the *3/2* mode grows to a large amplitude, the electron density flattens around the resonant surface as shown in Fig. 1. During island growth the situation can be however more complex. For the parameters of the red curves in Fig. 2 (left), Fig. 3 shows the radial profiles of the *m/n=0/0* component of the plasma current density (left), the safety factor (middle), and the *0/0* component of the electron density (right) at $t=0$ and $0.001\,\tau_R$. There is a strong perturbation in the plasma current density around the $q=3/2$ surface due to the mode coupling and low plasma resistivity, similar to that observed in the calculations of plasma response to externally applied RMPs [4], causing the flattening of the local q-profile at $q=3/2$ surface. The electron density decreases at $r_{3/2}$ but increases on its two sides.

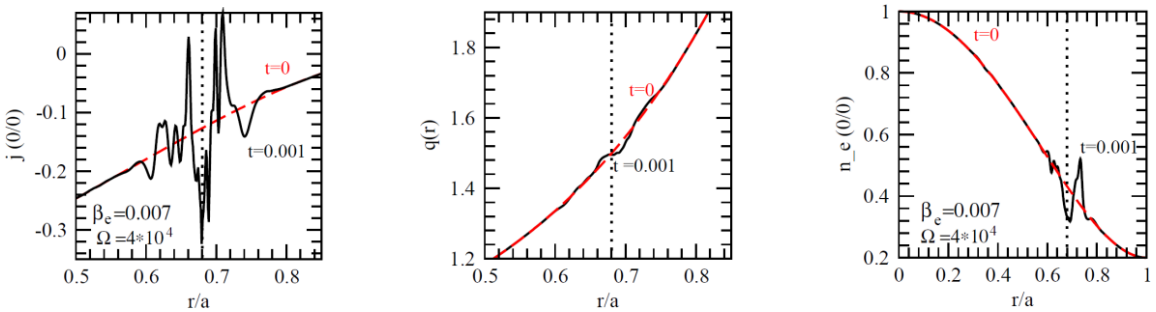

FIG. 3. For the parameters of the red curves in Fig. 2 (left), radial profiles of the m/n=0/0 component plasma current density (Left), the safety factor (Middle), and the m/n=0/0 component electron density $n_{e,0/0}$ (Right) at t=0 and $0.001\,\tau_R$.. The vertical dotted line shows $r_{3/2}$ location.

For a sufficiently high value of Ω but a moderate β_e, the *3/2* mode saturates at a small amplitude, while the originally unstable *2/2* mode is suppressed by its coupling to the *3/2* mode. As an example, the time evolution of the normalized *2/2* (dotted curves) and *3/2* (solid) island widths are shown in Fig. 4 (left) with $\Omega=4\times10^4$ for $\beta_e=0.005$ (blue) and *0.006* (red), being slightly lower than that for the red curves in Fig. 2 (left). The time evolution of a single *2/2* mode is also shown (dashed). The *3/2* island saturates at a small width of about *0.01a*, while the *2/2* mode growth is suppressed by its coupling to the *3/2* mode. Radial profiles of the normalized $\psi_{2/2}$ (black) and $\psi_{3/2}$ (red) at $t=2.8\times10^{-3}\,\tau_R$ are shown in Fig. 4 (right) for $\beta_e=0.006$. The $\psi_{2/2}$ profiles have the feature of an ideal mode, while the $\psi_{3/2}$ profiles have the feature of a tearing mode.

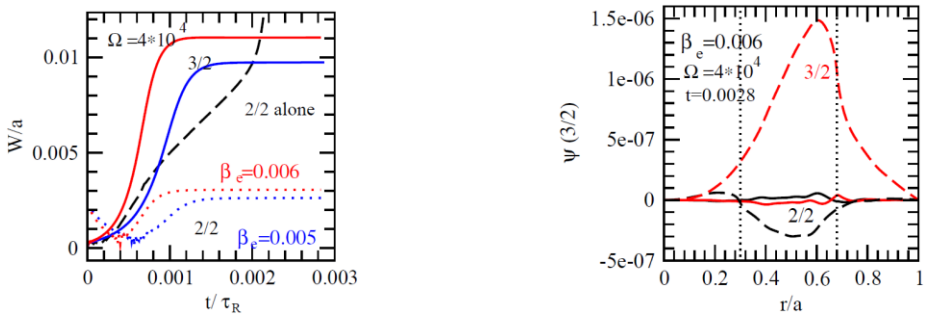

FIG. 4. (Left) Time evolution of the normalized 2/2 (dotted curves) and 3/2 (solid) island widths for β_e=0.005 (blue) and 0.006 (red) with Ω=4×10^4. The dashed curve refers to a single 2/2 mode. (Right) Radial profiles of the normalized $\psi_{2/2}$ (black) and $\psi_{3/2}$ (red) for β_e=0.006 at t=2.8×10^{-3} τ_R. The solid (dashed) curves show the real (imaginary) parts. The locations of q=1 and 3/2 surfaces are marked by vertical dotted lines.

In the following, the *m/n=1/1* mode and its harmonics, *2/2*, *3/3*, …, are additionally included in calculations. This allows for the growth of internal kink modes and sawtooth crashes, as shown in Fig. 5 (left) for the parameters: Ω=2×10^4, β_e= 0.005, $D_\perp$=0.376 (a^2/τ_R), f_b=0.13 at $r_{q=1}$ and f_b=0.4 at $r_{3/2}$. The sawtooth crash at $t=2\times10^{-5}\,\tau_R$ results in a sudden decrease (increase) of the normalized *m/n=0/0* component of the electron density inside (outside) the original *q=1* surface at $r_{q=1}=0.3a$ and a flattening of the q-profile in the central region to about unity. Corresponding radial profiles of the normalized *m/n=0/0* component of the electron density are shown in Fig. 5 (middle). It has a local perturbation around $r_{3/2}$ at $t=9.9\times10^{-5}\,\tau_R$, similar to that in Fig. 3. In a later time the *3/2* mode grows up to a large amplitude, and the electron density flattens around $r_{3/2}$, similar to what is shown in Fig. 1.

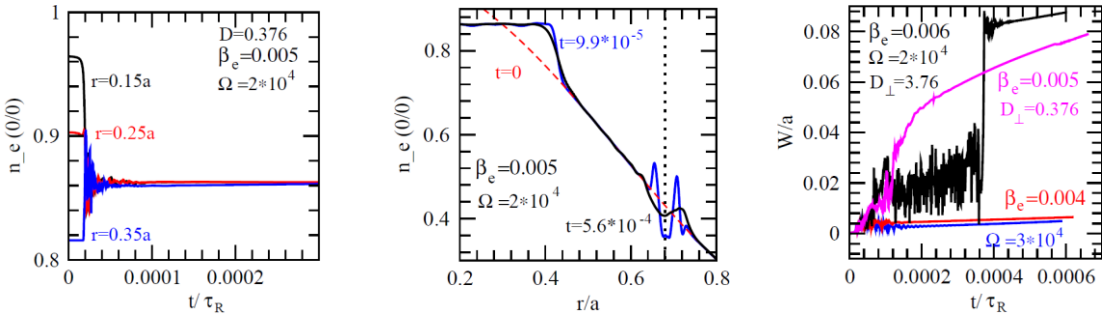

FIG. 5. (Left) Time evolution of the normalized m/n=0/0 component of the electron density at r=0.15, 0.25 and 0.35a for Ω=2×10^4, $D_\perp$=0.376 (a^2/τ_R), and β_e=0.005. The sawtooth crash happens at $t=2\times10^{-5}\,\tau_R$. (Middle) Corresponding radial profiles of the normalized m/n=0/0 component of the electron density at t=0, 9.9×10^{-5} and 5.6×10^{-4} τ_R. The vertical dotted line shows the $r_{3/2}$ location. (Right) Corresponding time evolution of the 3/2 island width (magenta curve). The black (red) curve is obtained with a larger particle diffusion coefficient ($D_\perp$=3.76 a^2/τ_R) for β_e=0.006 (0.004). The blue curve is obtained with Ω=3×10^4, keeping other input parameters the same as those for the black one.

The corresponding time evolution of the *3/2* island width is shown in Fig. 5 (right) by the magenta curve. After the sawtooth collapse, the *3/2* mode first oscillates at a low amplitude *(W/a~0.01)* around $t=10^{-4}\,\tau_R$ but grows afterwards. Compared to the case of a long-lived 2/2 mode triggering a 3/2 island (black curve of Fig. 2 (left)), a higher β_e value is required for the *3/2* island to grow up after sawtooth crash. For the latter case, the *2/2* perturbation is large only during the sawtooth collapse but becomes much smaller afterwards. The black curve demonstrates the stabilizing effect of a faster particle transport ($D_\perp$=3.76 a^2/τ_R), otherwise the

same parameters as for the magenta curve (except for $\beta_e=0.006$). With a larger value of $D_\perp$, the *3/2* island first oscillates at $W \sim 0.01\text{-}0.02a$ before $t=3.6\times10^{-4}\,\tau_R$ and grows up much later. Keeping the other input parameters as for the black curve, the *3/2* mode remains at a very small amplitude for a lower value of β_e, $\beta_e=0.004$ (red), or a higher value of Ω, $\Omega=3\times10^4$ (blue), indicating the destabilizing (stabilizing) role of a larger β_e (dimagnetic drift).

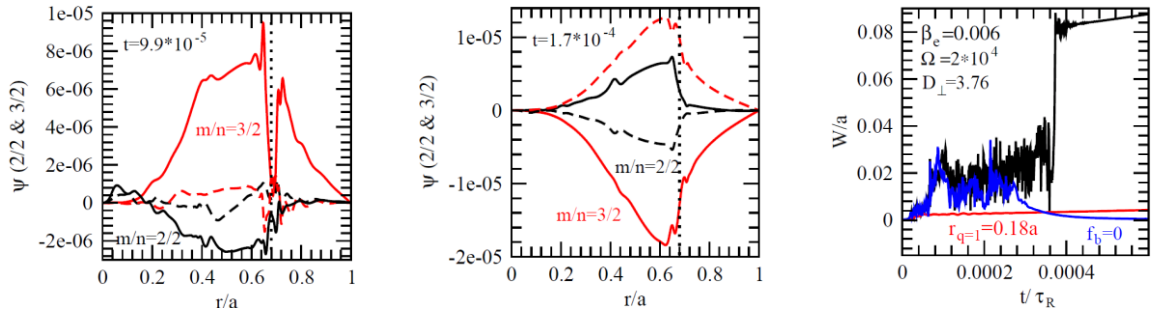

FIG. 6. (Left and Middle) Corresponding to the case shown in Fig. 5 (left), radial profiles of the normalized $\psi_{3/2}$ (red curves) and $\psi_{2/2}$ (black) at $t=9.9\times10^{-5}\,\tau_R \sim 2.3$ms and $1.7\times10^{-4}\,\tau_R \sim 3.9$ms are shown. The solid (dashed) curves correspond to the real (imaginary) parts. (Right) The black curve is the same as that in Fig. 5 (right). The red curve is obtained for an upwards shifted equilibrium q-profile ($r_{q=1}= 0.18a$), and the blue curve is for zero bootstrap current, with the other input parameters the same as for the black curve.

Corresponding to Fig. 5 (left), the radial profiles of $\psi_{3/2}$ (red curves) and $\psi_{2/2}$ (black) are shown at $t=9.9\times10^{-5}\,\tau_R \sim 2.3$ms and $1.7\times10^{-4}\,\tau_R \sim 3.9$ms in Fig. 6 (left and middle). The $\psi_{3/2}$ profiles again first have the feature of an ideal mode, but the $n=2$ perturbations are not shielded by the $q=1.5$ surface. Later in time, the $\psi_{3/2}$ profiles have the feature of a tearing mode once the mode amplitude becomes large, similar to what was shown in Fig. 2.

A sufficiently large sawtooth crash amplitude and bootstrap current density are required for the *3/2* island to grow to a large amplitude, as seen in Fig. 6 (right). The black curve is the same as that in Fig. 5 (right), shown here for comparison. If the bootstrap current is taken to be zero (blue), the *3/2* mode first oscillates around $W\sim0.01a$ and then decays. When using an upwards shifted equilibrium q-profile with a smaller $r_{q=1}$, $r_{q=1}= 0.18a$, and therefore a smaller sawtooth crash amplitude, the *3/2* mode remains at a low amplitude even with the bootstrap current included (red).

4. Effect of Static RMPs on Small Magnetic Island Growth

The toroidal mode coupling is neglected in this section. Instead, an external static RMP of m/n component is applied, taken into account by a modified boundary condition

$$\psi_{m/n}|_{r=a} = \psi_{a,m/n}\, aB_{0t}\cos(m\theta+n\phi), \qquad (6)$$

where $\psi_{a,m/n}$ is the normalized amplitude of the *m/n* component of the perturbed flux at $r=a$. A monotonic q-profile is used with the $q=2$ surface located at $r_{2/1}=0.628a$. The equilibrium electron density has a parabolic radial profile. The electron diamagnetic drift frequency is $\omega_{*e0}=1.5\times10^5/\tau_R$ ($f_{*e0}=1$ kHz) at $r_{2/1}$ for $\Omega=2\times10^4$. Other input parameters are: $f_b=0.35$, $a/R_0=0.294$, $D_\perp=\mu/5$ and $\mu_e=0$. Without applying RMPs, the *m/n=2/1* magnetic island is unstable even for $f_b=0$ and saturates at a width of $0.2a$.

The normalized (to ω_{*e0}) equilibrium electron fluid rotation frequency at $r=r_{2/1}$ can be defined as $\omega_n\equiv(1-\omega_0)$, where $\omega_0\equiv-\omega_{E0}/\omega_{*e0}$, and ω_{E0} is the frequency due to $\boldsymbol{E}\times\boldsymbol{B}$ plasma

rotation. For a static RMP with $\Omega=2\times10^{4}$ and $\omega_n=-3.5$ ($\omega_0=4.5$), corresponding to a plasma rotation in the ion drift direction with a frequency being 4.5 times larger than $|\omega_{*e0}|$, the time evolution of the 2/1 island width is shown in Fig. 7 (left). The island grows for small ($\psi_{a,2/1}=0,\ 7\times10^{-5}$) or large ($\psi_{a,2/1}=6\times10^{-4}$) external perturbations, but saturates at a small amplitude for $\psi_{a,2/1}=8\times10^{-5}$ - 5×10^{-4}.

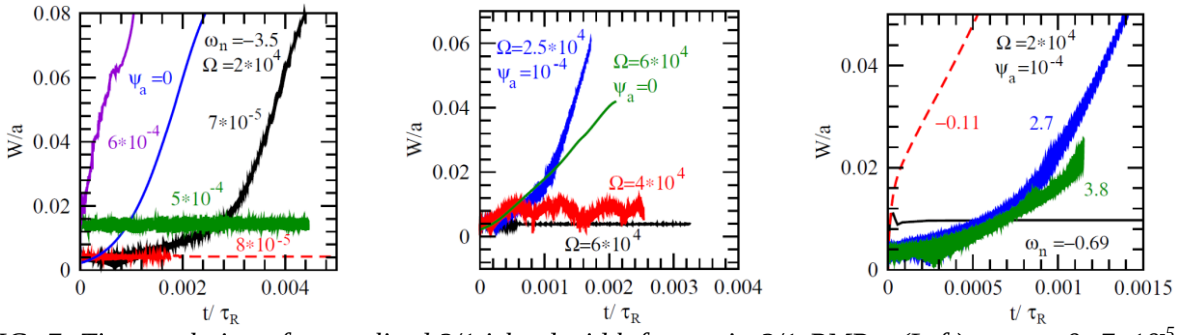

FIG. 7. Time evolution of normalized 2/1 island width for static 2/1 RMPs. (Left) $\psi_{a,2/1}=0,\ 7\times10^{-5}$, 8×10^{-5}, 5×10^{-4}, and 6×10^{-4} for $\Omega=2\times10^{-4}$ and $\omega_n=-3.5$. (Middle) $\Omega=2.5\times10^{-4}$, 4×10^{-4} and 6×10^{-4} for $\omega_{E0}=-2.6\times10^{5}/\tau_R$ and $\psi_{a,2/1}=10^{-4}$. The green curve is for $\Omega=6\times10^{-4}$ and $\psi_{a,2/1}=0$. (Right) $\omega_n=-0.69$, -0.11, 2.7 and 3.8 for $\Omega=2\times10^{-4}$ and $\psi_{a,2/1}=10^{-4}$.

For the plasma rotation in the electron drift direction (with $\omega_{E0}=-2.6\times10^{5}/\tau_R$), the island evolution with various values of Ω is shown in Fig. 7 (middle) for a static external perturbation of $\psi_{a,2/1}=10^{-4}$. The island grows for $\Omega=2.5\times10^{-4}$ ($\omega_n=2.3$) but doesn't for $\Omega=4\times10^{-4}$ or larger, indicating that a sufficiently large value of ω_{*e0} is required for suppressing the island growth. Similar trend is also found for the plasma rotation in the ion drift direction.

The island suppression by static 2/1 RMPs is asymmetric on the two sides of $\omega_n=0$, being more effective for $\omega_n<0$, as shown in Fig. 7 (right) for various values of ω_n with $\Omega=2\times10^{-4}$ and $\psi_{a,2/1}=10^{-4}$. This asymmetry is probably caused by the difference of the ion polarization current on the two sides of $\omega_n=0$. Such an asymmetry was also found in field penetration experiments [8]. Rotating 2/1 RMPs of a sufficiently high frequency is found to stabilize the 2/1 island growth even for zero electron fluid velocity, and the RMP rotates in the electron drift direction is more efficient for the stabilization.

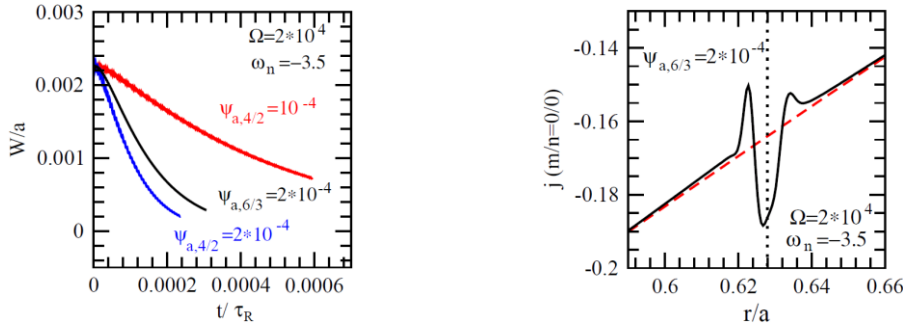

FIG. 8. (Left) Time evolution of the normalized 2/1 island widths with $\Omega=2\times10^{-4}$ and $\omega_n=-3.5$ by applying static m/n=4/2 or 6/3 RMPs. (Right) Corresponding radial profiles of the normalized m/n=0/0 component of the plasma current density at t=0 (dashed curve) and 2.8×10^{-4} (solid) for $\psi_{a,6/3}=2\times10^{-4}$ and $\omega_n=-3.5$.

Not only an external perturbation of the same (2/1) mode numbers is able to suppress magnetic islands, but also higher harmonics such as *m/n=4/2* or *6/3*. Again, a sufficient relative velocity between the local electron fluid and the external perturbation field is required. The corresponding time evolution of the *2/1* island width is shown in Fig. 8 (left) for $\Omega=2\times10^{-4}$ *and* $\omega_n=-3.5$ with different mode numbers of the applied RMP, *m/n=4/2* or *6/3*. In these examples the reason for the stabilizing effect is the change of the local equilibrium plasma current density gradient at *q=2* surface [4], which is also stabilizing for a sufficiently large plasma rotation velocity in addition to the diamagnetic drift and associated ion polarization current. An example is given in Fig. 8 (right) for the case of applying an *m/n=6/3* RMP, showing the local radial profiles of the normalized *m/n=0/0* component plasma current density at *t=0* (dashed curve) and 2.8×10^{-4} (solid) for $\psi_{a,6/3}=2\times10^{-4}$ and $\omega_n=-3.5$. The revered (increased) current density gradient inside (outside) the *q=2* surface caused by RMPs is known to be stabilizing for NTMs.

5. Summary

In this paper (a) the triggering of NTMs by sawtooth crashes and (b) the effect of externally applied resonant magnetic perturbations on the growth of small magnetic island are studied numerically based on the four-field equations [1]. It is found that:

(a) Without including *n=1* perturbations in the calculations, the *3/2* mode is more easily destabilized by its coupling to a *2/2* tearing mode for a larger plasma β ($=\beta_e$ with cold ion assumption) value or smaller electron diamagnetic drift frequency, as expected. The *3/2* mode starts as an ideal mode at the 3/2 surface after its onset, while the *n=2* perturbations are however not shielded by the *q=3/2* surface. For a sufficiently large diamagnetic drift frequency and moderate β values, the *3/2* mode saturates at a low amplitude, while the originally unstable *2/2* mode is stabilized by its coupling to the *3/2* mode. Including *n=1* perturbations in calculations, the *3/2* mode is triggered after a sawtooth crash for a sufficiently large β value, sawtooth amplitude, or low electron diamagnetic drift frequency at the *q=3/2* surface. In this case, the 2/2 mode has a large amplitude only for a short time after the crash. If the bootstrap current density is also large enough, the *3/2* mode grows to a large NTM amplitude.

(b) If the local electron diamagnetic drift frequency and bi-normal electron fluid velocity at the *q=2* surface are sufficiently large, the *m/n=2/1* island growth is found to be suppressed by static *2/1* RMPs of moderate amplitude, even with a significant fraction of the local bootstrap current density. Static *m/n=4/2* or *6/3* RMPs are also found to stabilize the *2/1* island growth for a sufficiently large plasma rotation velocity.

[1] Hazeltine R.D. *et al* 1985 Phys Fluids **28** 2466.
[2] Hender T.C. *et al* Nucl. Fusion **32**, 2091 (1992).
[3] Hu Q. *et al* 2012 Nucl. Fusion **52**, 083011.
[4] Yu Q., Günter S. and Lackner K. 2018 Nucl. Fusion **58** 054003.
[5] Grimm R. C., Greene J.M. and Johnson J. L. Methods in Computational Physics, edited by Killeen J. (Academic Press, New York, 1976), Vol. **16**, p. 253.
[6] Strumberger E. and Günter S. 2017 Nucl. Fusion **57** 016032.
[7] Igochine V. *et al* 2014 Phys. Plasmas **21** 110702.
[8] Koslowski H.R., Liang Y., Krämer-Flecken A. et al 2006 Nucl. Fusion **46**, L1.